Journal of Nuclear Materials 386–388 (2009) 553–556

Contents lists available at ScienceDirect

Journal of Nuclear Materials

journal homepage: www.elsevier.com/locate/jnucmat

# New insights into the structure of ODS particles in the ODS-Eurofer alloy

M. Klimenkov *, R. Lindau, A. Möslang

*Institute for Materials Research I, Forschungszentrum Karlsruhe GmbH, Hermann-von-Helmholtz-Platz 1, 76344 Eggenstein-Leopoldshafen, Germany*

A B S T R A C T

An oxide dispersion-strengthened alloy with 0.35% yttrium oxide produced on the basis of Eurofer steel was characterised by analytical transmission electron microscopy using a 1 nm probe size and energy-dispersive X-ray analysis as well as electron energy loss spectroscopy. According to the analytical results, the ODS particles detected consist of two phases. Formation of a thin V–Cr–O-containing shell of 0.5–1.5 nm thickness around each ODS particle and presence of 5–12% Mn inside the $Y_2O_3$ phase were detected. This study suggests that the chemical composition of ODS particles and, hence, their dispersion might be influenced by minor alloying elements contained in the main matrix.



## 1. Introduction

In the past few years, oxide dispersion-strengthened (ODS) steels produced by mechanical alloying techniques attracted growing interest as regards structural applications in nuclear fission and fusion power plants. Use of ODS alloys instead of the presently considered reduced-activation ferritic–martensitic (RAFM) steels would allow for an increase in the operating temperature of blanket structures in future fusion power reactors by 100 K to ~650 °C [1]. Development, production, and characterisation of ODS alloys were performed all over the world by different work groups. Mainly pure $Y_2O_3$ [1,2] or $Y_2O_3$ + Ti [3], and Al [4] were chosen as constituents of the ODS particles. The additional elements lead to the formation of ODS particles, consisting of complex oxides, and, thus, influence their morphology, spatial density, and distribution. These parameters are of major relevance to the mechanical properties of the alloy.

Previous publications that described transmission electron microscopy (TEM) investigations of alloys containing $Y_2O_3$ ODS particles always reported the formation of single-phase $Y_2O_3$ dispersoids [5,6]. The formation of this phase was confirmed by structural investigations [5]. TEM investigations of the ODS particle–matrix interfaces reveal that ODS particles are in no case single $Y_2O_3$-phase dispersoids. Their composition was found to be more complex, as it had been expected. The analytical TEM investigations at 1 nm spatial resolution presented here clearly show that ODS particles have a complex shell/core structure. It can be assumed that alloying elements like V and Mn play an important role in the formation of ODS particles and possibly in their spatial distribution, as it was shown for Ti [7].

## 2. Experimental

The ODS-Eurofer alloy was prepared by mechanical alloying of the Eurofer 97 powder with 0.3% $Y_2O_3$ powder and a subsequent HIP process. The basic composition of Eurofer 97 powder was 8.9 wt% Cr, 1.1 wt% W, 0.21 wt% V, 0.14 wt% Ta, 0.42 wt% Mn, 0.06 wt% Si, 0.11 wt% C, and Fe for the balance. Information on preparation steps and mechanical properties of this alloy can be found in Ref. [1]. The TEM specimens were prepared by mechanical grinding of 3 mm disks down to 150 μm. The disks were then etched in a Tenupol-3 jet polisher with a 20% $H_2SO_4$ + 80% $CH_3OH$ solution as electrolyte. The samples were cleaned on both sides after preparation in an ion milling system for 3 min using an ion beam of 2900 V and 4° etching angle.

The investigations were performed using an FEI Tecnai 20F microscope equipped with a Gatan image filter for electron energy loss spectroscopy (EELS) as well as with a high-angle annular dark field (HAADF) detector for scanning TEM (STEM). The microscope was operated at 200 kV accelerating voltage with a field emission gun. The EELS experiments were performed in the STEM mode with a probe size of ~1 nm and a probe current of 0.1 nA ($6 \times 10^8$ e/s). The experimental conditions were chosen such that the collection semi-angle was 13 mrad and the beam convergence angle was 10.5 mrad. For EELS measurements, an energy resolution of 1.1 eV and dispersion of 0.1 eV/channel were employed.

## 3. Results and discussion

The composition of ODS particles inside the alloy was studied by both EDX/EELS line scan and 2-d mapping experiments. In Fig. 1, EDX maps of an area with two ODS particles, 24 and 14 nm in diameter, are presented. The particles show a darker contrast in the HAADF image (Fig. 1(a)) as well as in Fe and Cr maps (Fig. 1(b) and (c) and a brighter contrast in Y and O maps

* Corresponding author.
*E-mail address:* michael.klimenkov@imf.fzk.de (M. Klimenkov).

0022-3115/$ - see front matter © 2009 Elsevier B.V. All rights reserved.
doi:10.1016/j.jnucmat.2008.12.174

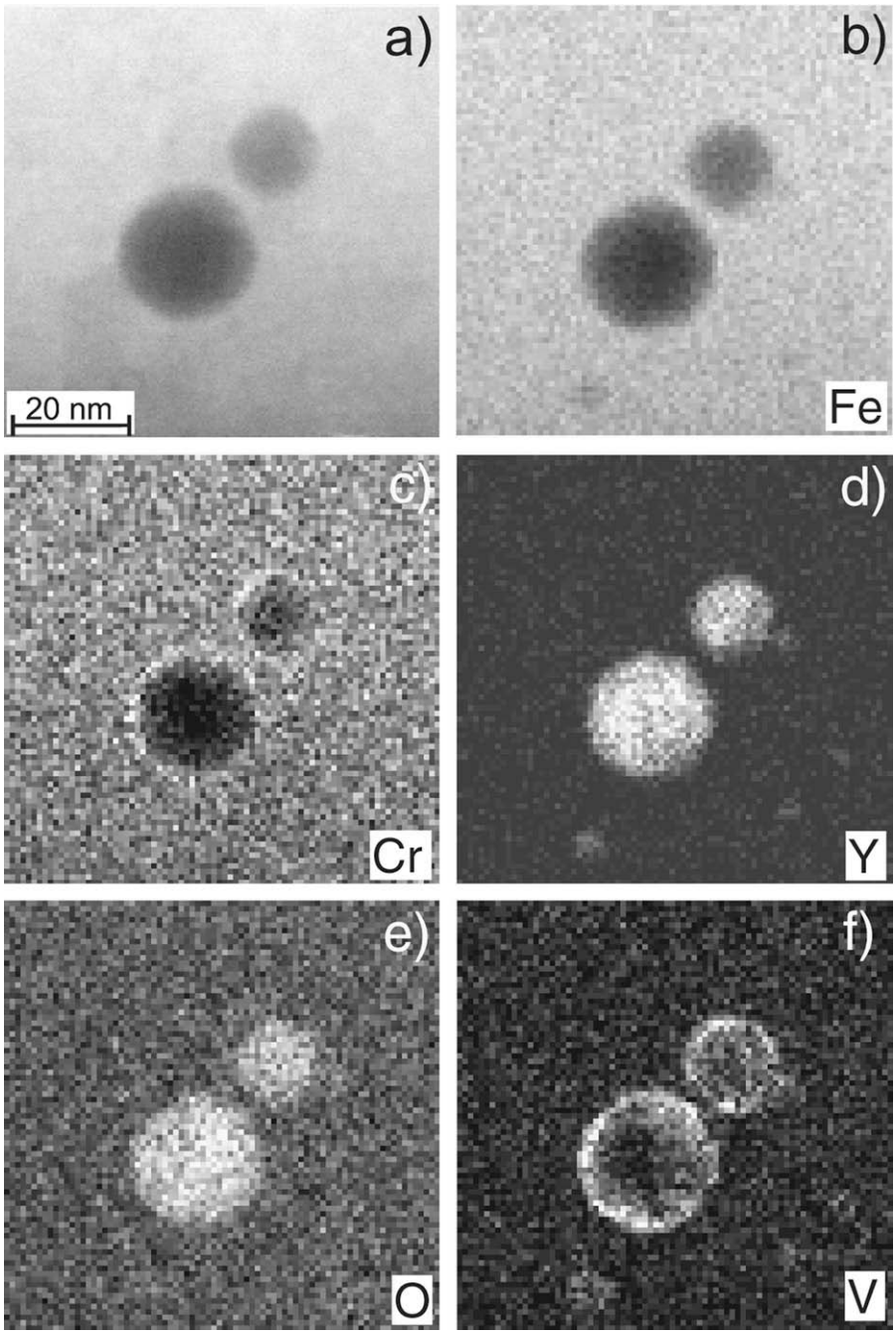


**Fig. 1.** EDX elemental mapping of an area with two ODS particles: (a) HAADF image, (b)–(f) elemental maps obtained using Fe-Kα, Cr-Kα, Y–L, O–K, and V-Kα EDX lines, respectively.

(Fig. 1(d) and (e)). The V-rich shell around both particles is clearly visible in the V map (Fig. 1(f)). A slight increase of the Cr concentration around ODS particles can be observed in the Cr map (Fig. 1(c)). Comparison of Cr-Kα line intensity in the region near the ODS particle with the average in the matrix shows an increase of the Cr concentration from 9 to 12–15 mass percent. These measurements clearly reveal the formation of an almost uniform shell around the ODS particle with a (V, Cr) composition. Taking into account a three dimensional shell structure, the shell thickness was estimated to amount to 1.0–1.5 nm.

The application of EELS clearly proves the presence of Mn inside each ODS particle. In Fig. 2, the results of spatially resolved EELS investigations are presented. The EELS spectra were obtained, while the electron beam scanned through the ODS particle of 11 nm size. The particle is displayed in Fig. 2(a). The 30 EELS spectra in the range from 500 to 760 eV are presented in Fig. 2(b). The V–$L_{2,3}$, O–K, Cr–$L_{2,3}$, Mn–$L_{2,3}$, and Fe–$L_{2,3}$ edges are clearly visible in the spectra. The V–$L_{2,3}$ and Mn–$L_{2,3}$ edges are only detectable in the ODS particle, but not in the matrix. The intensity of the V–$L_{2,3}$ edge increases at the edges of the ODS particle, indicating a V-rich shell. The O–K EELS edge has a fine structure that is typical of $Y_2O_3$ material. The intensity of this edge is not zero in the regions outside of the ODS particle due to the oxidation of the specimen surface. Using the cross-section scattering ratio of 1.8 for Mn–$L_{2,3}$ and O–K EELS edges [8], the Mn/O ratio was estimated to range from about 0.05 to 0.10. From this, a $(Y_{1.8}Mn_{0.2})O_3$ composition of this

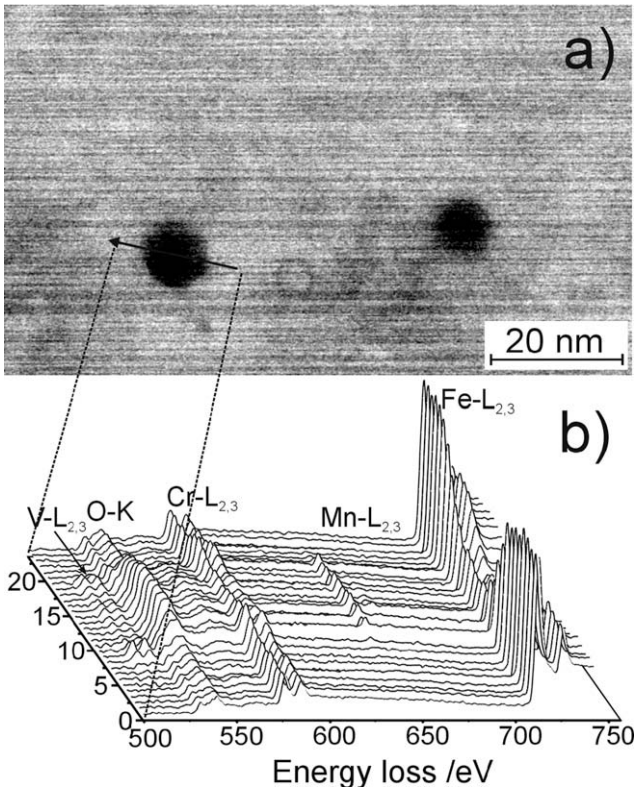


**Fig. 2.** Spatially resolved EELS investigations of ODS particles. The area with two ODS particles is imaged in (a). The series of EELS spectra obtained while scanning along the marked line is presented in (b).

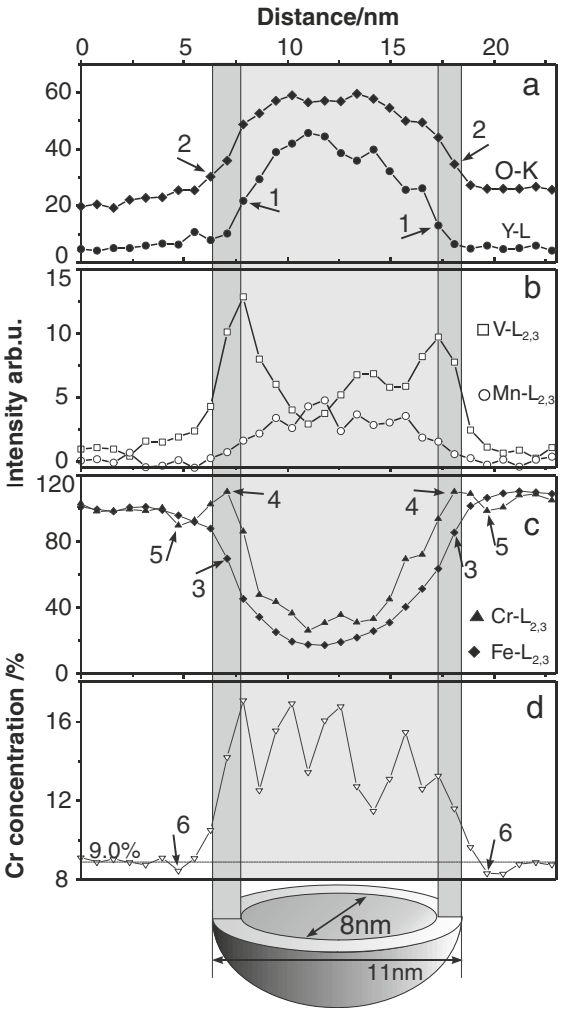


**Fig. 3.** The intensity profiles of EDX lines and EELS edges. Part (a) gives O and Y profiles, part (b) V and Mn, and part (c) Cr and Fe. Part (d) presents the normalised Cr concentration.

ODS particle can be derived. Earlier analytical investigations performed using the EDX method did not detect any Mn inside ODS particles, because Mn-Kα and Mn-Kβ lines overlapped with Cr-Kβ and Fe-Kα lines – the main alloying elements.

The intensity profiles of the EELS elemental edges and EDX lines shown in Fig. 2 are presented in Fig. 3(a)–(d). Their detailed analysis allows for a precise determination of the elemental distribution and conclusions with respect to the location of different phases, the $Y_2O_3$ core, and V, Cr shell on the nanometer scale.

The size of the $Y_2O_3$ core was determined from the curve pattern of the Y–L EDX profile (Fig. 3(a)). The points of the Y–L curve marked by arrow No. 1 show a pronounced increase in Y intensity compared to the background. The distance between these points of 8 nm is the $Y_2O_3$ core size. The increase of the O–K signals starts about 1–1.5 nm before the Y–L signal (marked by arrow No. 2). This clearly indicates that the oxide phase is 2–3 nm larger in diameter than the $Y_2O_3$ core. The V–$L_{2,3}$ profile shows the same pattern as the O–K curve in the region close to the ODS particle/matrix interface and reaches its maximum value in the interface area between the $Y_2O_3$ core and the shell (Fig. 3(b)). The intensity of the V–$L_{2,3}$ edge remains weak, but detectable by scanning through the $Y_2O_3$ core. This behaviour corresponds to the presence of a V-rich shell around the ODS particle. The intensity of the Mn–$L_{2,3}$, edge remains approximately constant in the entire $Y_2O_3$ phase. Its presence in the shell cannot be proven definitely due to the weak intensity of the Mn edge. It can only be supposed that Mn is dissolved in the $Y_2O_3$ phase.

The increasing Cr concentration around the particle, which was detected by EDX mapping, is clearly visible in the Cr and Fe profiles (Fig. 3(c)). Both profiles were normalised, such that intensities of Cr–$L_{2,3}$ and Fe–$L_{2,3}$ edges were assumed to be 100 for the matrix. In Fig. 3(d), the variation of the normalised Cr concentration in the matrix, related to the Fe signal as reference, is presented. In the areas located 3–4 nm from ODS particle, the Fe and Cr concentrations do not change. The Fe concentration shows a decrease of about 70% as the beam scans through the shell of ODS particle (arrow No. 3). The normalised Cr concentration increases at the same points from 9.0% to 11–14% (arrow No. 4). While scanning through the ODS particle, the Cr concentration varied from 14% to 18% and, hence, was 40–70% higher than the matrix average (Fig. 3(d)). At the points marked by arrow No. 5 in Fig. 3(c) and No. 6 in Fig. 3(d), a small reduction of the Cr concentration to 8.2% can be observed clearly. The diffusion of Cr into the shell might be the possible reason for the formation of this Cr-depleted area. The existence of this area in the prepared material allows conclusions to be drawn with respect to the formation mechanism of the shell around the ODS particle. It is generally suggested that the ODS particles and the shell form during hot isostatic pressing at 1150 °C or during subsequent cooling, because several TEM studies of mechanically alloyed powder do not show the presence of ODS particles. The existence of this Cr-depleted area might indicate that this shell and the 'depleted area' were formed in the cooling stages, when the thermally activated Cr diffusion was not sufficient to minimise these concentration differences even in the area of a few nanometers. It can be suggested that this temperature is below 850 °C, where Cr diffusion is strongly reduced.

The detailed analysis of the elemental profiles confirms the formation of a (V, Cr) oxide layer of 1–2 nm thickness around the $Y_2O_3$ core. Due to the small thickness and the embedding in the matrix, this analysis does not supply any quantitative information on the exact composition of the shell. This layer was detected in all the ODS particles investigated. It may be supposed that the layer is not always continuous. Its thickness can vary from 0.2–0.4 nm, which is hardly detectable in line scan experiments, to 2.5 nm. In many cases, only the application of EELS measurements to the V–$L_{2,3}$ edge allows for detecting V presence at the $Y_2O_3$/matrix interface. Such thin layers are not detectable by the EDX method which generally is less sensitive than EELS. The EELS investigations at 250–450 eV energy did not indicate any presence of nitrogen inside the shell.

Both V and Mn are minor alloying elements in the steel with a content of 0.21 wt% and 0.49 wt%, respectively. Their presence effectively influences the mechanical properties. Vanadium, for example, is a strong carbide former and is commonly added to the steels for grain refinement and hardening [9]. The concentration of these two elements in the matrix is reduced by trapping at the ODS particles. It may be supposed that the depletion of the matrix could have a negative influence on strength and ductility of the steel. On the other hand, Mn and V as compositional elements of the ODS particles are expected to influence their formation and stability as well as their size and spatial distribution. By the formation of a V, Cr oxide shell around the ODS particles, excessive oxygen is gettered, which may have a positive effect on the mechanical properties. The effects on the mechanical properties have not yet been quantified. Further investigations of different batches subjected to different production routes and thermal treatments with respect to their microchemical composition and ODS particle distribution are necessary. To really understand the mechanisms, further theoretical considerations and modelling could be helpful.

## 4. Conclusion

Analytical TEM investigations were applied to study the chemical composition of ODS particles inside the ODS-Eurofer alloy. The investigations prove that the ODS particles have a complex structure. The core of the ODS particle consists of a $(Y_{1.8}Mn_{0.2})O_3$ phase and is surrounded by a 0.5–1.5 nm V, Cr oxide layer. As it was shown earlier, the $(Y_{1.8}Mn_{0.2})O_3$ phase exhibits a typical cubic $Y_2O_3$ structure with $a = 1.06$ nm. The formation of this shell was detected around each ODS particle investigated. The complex composition of ODS particles leads to the assumption that their dispersion and distribution might be influenced by the Mn and V concentrations in the matrix.

## References

[1] R. Lindau, A. Moslang, M. Schirra, P. Schlossmacher, M. Klimenkov, J. Nucl. Mater. 307–311 (2002) 769.
[2] C. Cayron, E. Rath, I. Chu, S. Launois, J. Nucl. Mater. 335 (2004) 83.
[3] M.K. Miller, K.F. Russell, D.T. Hoelzer, J. Nucl. Mater. 351 (2006) 261.
[4] M. Klimiankou, R. Lindau, A. Moslang, J. Schröder, Powder Metall. 48 (3) (2005) 277.
[5] M. Klimiankou, R. Lindau, A. Möslang, J. Cryst. Growth 249 (1&2) (2003) 381.
[6] N. Baluc, R. Schaublin, P. Spätig, M. Victoria, Nucl. Fus. 44 (2004) 56.
[7] S. Ohtsuka, S. Ukai, M. Fujiwara, T. Kaito, T. Narita, J. Phys. Chem. 66 (2005) 571.
[8] F. Hofer, P. Golob, Micron Microsc. Acta 19 (1988) 73.
[9] R. Lagneborg, T. Siwecki, S. Zajac, B. Hutchinson, Scand. J. Metall. 28 (1999) 186.